Imperfect Fabry-Perot resonators

Klaassen, T.

CHAPTER 9

Combining a stable and an unstable resonator

We investigate a two-mirror resonator comprising two multi-mode cavities that are intrinsically coupled. The key element of this system is a mirror with a combined convex inner part and a concave shell. Tuning of the cavity length allows us to study the coupling inside a stable-unstable cavity combination as well as inside a stable-stable combination. The former configuration is expected to show the onset of chaos.

9.1 Introduction

In this Chapter, we present a preliminary experimental investigation of a novel type of open optical resonator that may show chaos. Wave chaos has been demonstrated in the microwave regime in closed billiards in 1990 [91]. In the optical regime, wave chaos is very hard to obtain with closed resonators since omnidirectional perfectly reflective coatings (as metals are in the microwave domain) do not exist. Furthermore, such closed resonators would be hard to access and adjust. On the contrary, a standard *open* resonator consisting of two high-reflectivity laser mirrors does not suffer from these problems, but such a configuration does not normally lead to chaos.

Two requirements have to be fulfilled for chaotic behavior in a resonator, be it closed or open. First, optical paths in a resonator have to be exponentially sensitive to the initial conditions and, secondly, the light has to be confined inside the cavity for a sufficiently long time, to produce mixing. A two-mirror unstable resonator offers the exponential sensitivity, but the rays escape the cavity after only a few round-trips so that mixing does not occur. A two-mirror stable resonator can confine the light, but is an imaging systems that does not possess the exponential sensitivity. To combine the "best of both worlds", we have designed the composite mirror shown on the right-hand sides of the two cavities shown in Fig. 9.2, below. This special composite mirror has a convex center and a concave outer part; it will also be denoted as a "bifocal" mirror as it contains two radii of curvature and thus two foci. While the unstable inner cavity provides the exponential sensitivity, the outer cavity collects the light leaving the unstable cavity and injects it back into the inner cavity, thus fulfilling the mixing requirement.

Numerical simulations help us to determine the proper configuration which might show chaos. *Wave* chaos for our configuration can, however, not be shown numerically, as in practice the wave equation can only be solved for small systems with a typical dimension a and wavenumber k, where $ka < 150$ [92, 93]. The experimental cavity, presented in this Chapter, corresponds to $ka \sim 8000$. Although our experiment deals with waves, the demonstration of *ray* chaos is important as ray chaos is a requirement for wave chaos, *i.e.*, when a resonator does not exhibit *ray* chaos, *wave* chaos will not occur either [42]. The presence of *ray* chaos in an open optical 2D-resonator has been predicted by Aiello *et al.* [79] based on calculations of the Lyapunov exponent. The Lyapunov exponent [94] is a measure for the exponential sensitivity to the initial conditions; it characterizes the mean rate of exponential divergence between two nearby orbits. The strip-resonator proposed by Aiello *et al.*, shown in Fig. 9.1, is a stable symmetrical two-mirror cavity in which a third two-side convex mirror is placed in the middle. For practical reasons this configuration has been slightly modified; the convex part has been combined with the concave outer mirror.

The most promising configuration to observe chaos does not only show a high Lyapunov exponent, but also a sufficient confinement of the rays inside the resonator. To allow sufficient time for chaos to develop, the ray should stay inside the resonator longer than the time associated with the Lyapunov exponent; $\tau_{\text{Lyapunov}} < \tau_{\text{escape}}$. Numerical simulations of the 2D cavity have been performed [95] for various cavity lengths and radii of curvature of the bifocal mirror. The most promising configuration, which will be introduced in Section 9.2, shows that it takes on average 1.5 round-trips [95] to show exponential divergence. The time a ray stays inside the resonator τ_{escape} is determined by the transmission loss due to the finite

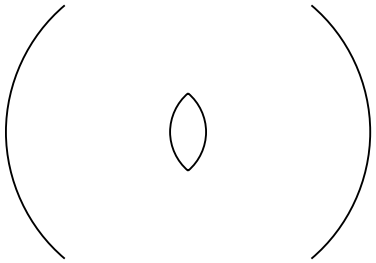

Figure 9.1: *Two-mirror cavity in which a third two-side convex mirror is placed in the middle. The inner mirror in combination with one of the outer mirrors forms an unstable resonator, whereas the combination of both outer mirrors forms a stable resonator.*

reflectivity of the mirrors and the escape or diffraction loss due to the finite transverse dimensions of the mirrors. The former is simply determined by the quality of the mirror coating, and will be discussed below. The latter is primarily determined by the aspect ratio of the resonator. Numerical simulations show that a square configuration ($L \sim 2b$) minimizes the escape of rays caused by the open nature of our cavity. Due to the ray character of the simulations only relative dimensions L/b are important. In contrast, when the wave character of light is taken into account, the absolute dimensions become important via the Fresnel number $b^2/\lambda L$, where b is the radius of the mirror, λ the wavelength, and L the cavity length.

The key characteristic of wave chaos is the repulsion between eigenfrequencies. To demonstrate this experimentally, it is necessary that resonances in the spectrum can be resolved, *i.e.*, the spectral width of a resonance should be small as compared to the average mode spacing, being the free spectral range divided by the number of modes. For confined modes, the spectral width is expressed by the cavity finesse $F = \pi/(1-R)$, which is fully determined by the reflectivity of the mirrors R. The number of "confined" modes in a stable resonator scales with the cavity dimensions and approximately equals the Fresnel number $N_F = b^2/\lambda L$. The eigenmodes can thus only be resolved when the Fresnel number is smaller than the finesse, which is realistically about 1000. This means that for a square cavity configuration and $\lambda = 800$ nm, the typical dimensions of the cavity should be in the order of $2b \approx L \approx 1$ mm.

The simulations provide only a simplified picture of reality. First of all, a realistic resonator is 3D and not 2D, as is assumed in the numerical simulations. In our experimental 3D-system, for instance, many (corkscrew-like) orbits exist that do not hit the dimple, *i.e.*, the convex central part of the bifocal mirror, at all. This means that in 3D the average number of round-trips needed to develop chaos will increase, as compared to the 2D-simulations. Furthermore, the experiment deals with waves, whereas interference effects are not taken into account in the numerical simulation. Therefore, although ray-simulations give us some insight, only an experiment can be conclusive on the existence of chaos.

To place our experiment in a broader historical perspective, we mention here some other experiments. One of the first experiments to describe the coupling of two resonators, is the coupling of two maritime clocks by Christian Huygens in 1662 [96]. He found that two nearby pendulum clocks swung with exactly the same frequency and 180 degrees out of phase. When he disturbed one pendulum the anti-phase state was restored within half an

hour. This simple experiment shows the essence of coupled systems. Examples are also found in the optical domain, *e.g.*, in ring-laser gyroscopes. In an ideal ring-laser, the two oppositely travelling waves are supposed to be uncoupled. Rotation of the resonator lets both waves experience a different path length and consequently different resonance frequency. This effect is known as the Sagnac-effect. If the intra-cavity light, however, experiences some backscattering (due to surface roughness and/or Fresnel reflection), coupling of the oppositely propagating waves is introduced [97] and the standing waves dominate at small rotation velocities. Also in optical systems with an active medium coupling can play a role. In dual VCSELs, two monolithic cavities are grown on top of each other and share a common mirror [98]. The degree of coupling is now determined by the quality of the transmission of the common mirror. Dual wavelength emission is generally observed.

In the system presented in this Chapter, both cavities are passive. Another difference as compared to other systems is the instability of the inner cavity. This accounts for the large coupling strength of both cavities. An uncoupled unstable resonator normally favors the lowest order modes, which is the least lossy, and operates (effectively) as a "single" mode-resonator. In our system the unstable resonator is, however, coupled to a stable resonator, which also supports the higher-order modes in the unstable cavity. Our system is thus a coupled multi-mode system, which makes it a very rich and intriguing system.

The general structure of this Chapter is as follows. In Section 9.2, the production method of the mirrors is discussed and both cavity configurations are introduced. A simple ray-tracing simulation of the cavity configurations, as presented in Section 9.3, pinpoints the most promising regimes. The experimental setup is discussed in Section 9.4. The rest of the Chapter is devoted to a study of the minimum requirements needed for chaos to be fulfilled. Questions that we will address experimentally are:

"Can we couple the inner and outer cavity?",

"How long does the light stay inside the cavity?",

"How often is the dimple hit?" and,

"Can the spectral resonances be resolved?".

These questions are answered on the basis of the two main methods at our disposal; spectral and spatial analysis. In Section 9.5, the experiments based on spectral information are introduced, while Section 9.6 presents and discusses the spatial intensity distributions on the mirror. All results are discussed in Section 9.7 and recommendations are made.

9.2 Substrates, mirrors and cavity configurations

The substrate for the composite mirror, with its concave outer part and convex inner part, can not be manufactured by traditional (polishing) methods. Diamond machining [67] does offer the possibility to produce such bifocal substrates, though. The substrates for the mirrors used in the experiment are made out of calcium fluoride (CaF_2). Calcium fluoride is a crystal widely used for optical substrates, *e.g.*, for lenses in lithography systems, as it has a high transmission at UV-wavelength, even below 175 nm [70]. The prime advantage of this material is that it chips very fine during the fabrication procedure so a low surface roughness ($\sigma_{RMS} \sim 2$ nm) can be achieved. Its melting temperature (1630 K) is much higher than the temperature reached during the high reflectivity coating process (~ 400 K); this implies that

the surface figure is maintained. Finally, it is transparent at 800 nm, which is the wavelength used in our experiment.

Two different pieces have been produced by TNO [31] according to our design; a concave and a bifocal one. The mirror substrates have been diamond machined with a chisel and the grooves on the substrate have a period ranging from $10-25$ μm. The concave mirror substrate has radii of curvature $R = 14$ mm and a nominal mirror radius $b = 1$ mm (see Fig. 9.2). The bifocal substrate has a radius of curvature $R = 14$ and $r = -3$ mm and a nominal mirror radius $b = 1$ mm and $a = 100$ μm, for the outer and inner part, respectively. Inspection of the composite mirror by an interferometer (WYKO-400) shows that the transition zone from the inner to the outer part is smaller than 15 μm and that the transition is smooth (step height$< \lambda/20$). We note that the inner and outer part of the composite mirror are automatically aligned and do not show tilt, as spheres always have a radius in common. For easy handling, the substrates have an outer radius of 3 mm, where the outer part with a radius r ranging from 1 to 3 mm, is machined conically to prevent this part from scattering light back into the resonator. Each diamond machined substrate, bifocal and simply concave, is mounted in a metal ring with an outer radius of 0.5 and 1 inch, respectively. We also possess a flat CaF_2-substrate with a diameter of 1 inch, which is not diamond machined but traditionally polished. All substrates are coated in the same coating run, with a stack of $12 \times 2 = 24$ layers of alternating Ta_2O_5 (refractive index 2.04) and SiO_2 (refractive index 1.46). The measured transmission of the mirrors after coating is 8×10^{-4}.

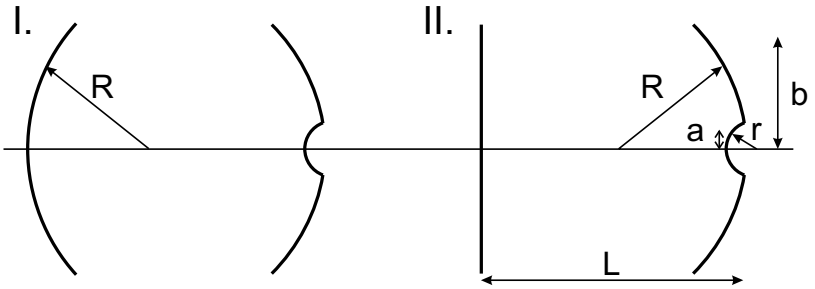

Figure 9.2: *Two cavity configurations, with an identical composite mirror on the right-hand side. The dimensions of the composite mirror are $R = 14$ mm, $r = -3$ mm, $a = 100$ μm, and b=1 mm. The left-hand mirror is either (I) concave with a radius of curvature $R = 14$ mm or (II) flat.*

Fig. 9.2 shows the two different cavity configurations that we have used; the dimple mirror in combination with the concave mirror (denoted in this Chapter as configuration I) and the dimple mirror in combination with the flat mirror (denoted as configuration II). The (radially) outer part of configuration I forms a resonator which is stable for all cavity lengths $L < 2R = 28$ mm. The stability of the inner cavity depends on the cavity length in a more complicated way and can be found from $0 \leq g_1 g_2 \leq 1$ [12], where $g_i = 1 - L/R_i$. Solving this equation for configuration I, where $R_1 = R = 14$ mm and $R_2 = r = -3$ mm, we find that the inner cavity is only stable for $11 < L < 14$ mm and thus unstable for $L < 11$ mm and $L > 14$ mm. This configuration has the advantage that we can explore the transition from a stable to an unstable inner resonator. Furthermore, we note that the magnification (equivalent

to the transverse mode stretching per round-trip) is limited to $M = 4.7$ for cavity lengths $L < 11$ mm (see Tab. 9.1).

When we replace the concave mirror by the flat one, we obtain configuration II which is equivalent to the geometry discussed by Aiello *et al.* [79]. It combines an outer part, which is stable for cavity lengths $L < R = 14$ mm, and an inner part, which is always unstable. Note that the magnification is already $M = 3$ for a cavity length of only $L = 1$ mm and increases with the cavity length, as shown in Tab. 9.2.

9.3 Ray-tracing the bifocal resonator

Extensive ray tracing simulations in ref. [95] have shown that ray-chaos is most likely found for $L \sim 2b$. In combination with the extra requirements for wave chaos, this condition becomes $L \sim 2b \lesssim 1$ mm [95]. In this Thesis a much simpler simulation is used to show how long the ray stays inside the resonator and how often the dimple is hit. The ray-tracing simulation, based on *ABCD*-matrix multiplication, calculates the path through the cavity for a given input position and injection angle on the bifocal mirror. A ray which hits the outer part of the mirror ($R = 14$ mm) experiences another *ABCD*-matrix than a ray that hits the inner part of the mirror ($r = -3$ mm).

To be able to perform some statistics, the path through the resonator is calculated for 51 input positions, equally spaced over the dimple (thus ranging from 0 to 100 μm), and 41 different angles (ranging from -0.01 to 0.01 rad) for every input position. These numbers are close to typical experimental values. The total number of injected rays is thus 2091. The number of round-trips is limited to 8000 (which would be equivalent to the unrealistically large cavity finesse $F = 2\pi \times 8000 \approx 50000$). From these data we calculate, for both configuration I and II, the probability distribution of the number of round-trips before escape from the resonator and of the number of dimple hits.

9.3.1 Configuration I

An overview of the simulations performed on a cavity I-configuration is shown in Tab. 9.1. It shows that outside the stable regime of the inner cavity, we hardly find stable orbits, except for the shorter cavity lengths. Only for very short cavity lengths, *e.g.*, $L = 1$ mm, most orbits stay inside the resonator for the maximized number of 8000 round-trips. This is also shown in more detail in Fig. 9.3a, where a probability distribution shows the number of rays vs. the number of round-trips before escape. The rays escaping earlier (less than 8000 round-trips) produce a (roughly) flat probability distribution. For the same cavity length, the average number of dimple hits is also substantial, 1548 out of 6694. The broad probability distribution shown in Fig. 9.3b indicates a variety of different orbits.

For $L = 12$ mm, the inner cavity of configuration I is stable and a ray remains on average inside the resonator for 4903 round-trips. We have to be careful with this number as rays can remain in the stable inner cavity without coupling to the outer cavity. Taking a closer look at the distribution of the number of round-trips a ray remains inside the cavity, we find that 60 % of the rays stay inside the resonator for all 8000 round-trips and that the other 40 % leave the cavity only after a few hits. The same division holds for the average number of dimple hits;

L [mm]	average # of round-trips	average # of dimple hits	N	M
1	6694	1548	8.3	2.6
2	1571	241	5.8	3.4
6	390	81	3.3	4.6
10	112	30	2.5	2.6
12	4903	4898	2.2	stable
15	80	12	1.9	-3.4

Table 9.1: *For six different lengths of a configuration I cavity, we have calculated both the average number of round-trips per ray before escape and the average number of dimple hits per ray. A total of* $41 \times 51 = 2091$ *different rays are traced through a configuration I-resonator, each over 8000 round-trips or less if the ray escapes at earlier time. The inner cavity is stable for* $11 < L < 14$ *mm. The numbers N and M are the degeneracy (*$= 2\pi/$*Gouy phase) and the magnification of the inner cavity, respectively.*

60 % of the rays hit the dimple every round-trip, whereas 40 % hit the dimple only a few times. This confirms our statement that most rays stay inside the stable inner cavity and that most other rays are lost. The stable inner cavity will not show chaos as a stable resonator is not exponentially sensitive to the initial conditions.

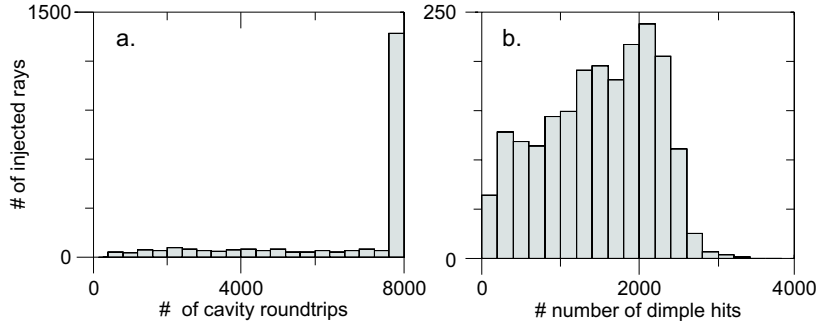

Figure 9.3: *Ray-tracing statistics for a configuration I resonator at a length of* $L = 1$ *mm with two concave mirrors (*$R = 14$ *mm), of which one has a central dimple (*$r = -3$ *mm). The two probability distributions show the number of rays (out of 2091) vs. (a) the number of round-trips before escaping and (b) the number of dimple hits.*

9.3.2 Configuration II

The statistics performed on configuration II is shown in Tab. 9.2. We again find that only for a very short cavity length a typical ray remains inside the cavity for a long time as well as a substantial number of dimple hits. Fig. 9.4 shows that for $L = 1$ mm only a fraction of the injected rays remain in the cavity for the full 8000 round-trips. Only for shorter cavity lengths, *e.g.*, $L = 0.5$ mm, almost all rays remain inside the cavity.

L [mm]	average # of round-trips	average # of dimple hits	N	M
0.5	7163	1477	16.5	2.2
1	2946	625	11.6	3.0
2	152	47	8.1	4.4
6	31	13	4.4	9.9

Table 9.2: *For four different cavity lengths of configuration II, we calculated both the average number of round-trips per ray before escape and the number of dimple hits per ray. A total of* $41 \times 51 = 2091$ *rays are traced through a configuration II-resonator, each over 8000 round-trips or less if the ray escapes at earlier time. The numbers N and M are the degeneracy (=*$2\pi/$*Gouy phase) and the magnifications of the inner cavity, respectively.*

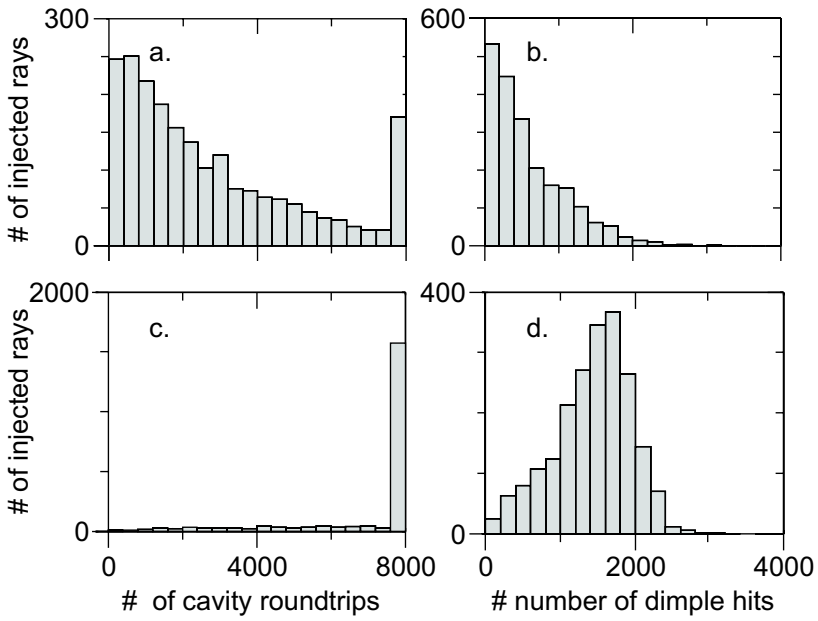

Figure 9.4: *Ray-tracing statistics for a configuration II-resonator at the cavity lengths* $L = 1$ *mm (upper figures) and* $L = 0.5$ *mm (lower figures). The probability distributions show the number of rays (out of 2091) vs. the number of round-trips before escaping (a) and (c) and vs. the number of dimple hits (b) and (d).*

9.4 The experimental setup

The two mirrors forming the cavity are mounted in stable top-actuated mounts (New Focus 9774 and 9775). A tunable Titanium Sapphire ring laser (Coherent 899-01), which is driven by a diode-pumped laser (Coherent Verdi) and operates at a wavelength of $\lambda = 800$ nm, is used to inject our cavity. A lens ($f = 10$ cm) in front of the cavity mode-matches the input beam to the lowest-order mode of the cavity. The cavity length is scanned with a piezo-element to obtain the transmission spectrum. Besides the spectral information also the intensity profile on the back-mirror is monitored with a CCD-camera behind the cavity.

For accurate tuning of the *relative* cavity length one mirror is placed on a translation stage (PI M-521). The *absolute* cavity length is found by using frequency-degenerate points of the stable cavity (see Chapter 5). These special points can be recognized easily, both spectrally and in the intensity profile on the mirror, as follows. At these N-fold frequency-degenerate points, spectral resonances overlap and form N clumps of modes, each spaced at $\Delta\nu_{\mathrm{FSR}}/N$, where $\Delta\nu_{\mathrm{FSR}}$ is the free spectral range. Furthermore, for off-axis injection at an angle N spots appear in the intensity profile on the mirror. As every N-fold frequency-degenerate point belongs to a unique cavity length (for the given radii of curvature of the mirrors), the absolute cavity length can be determined very accurately, up to a few μm.

9.5 Fabry-Perot spectra

9.5.1 Coupling the inner and outer cavity

Coupling of the inner and the outer cavity is needed to reinject light into the unstable inner cavity, where chaos can develop. To check if coupling is feasible, we operate a configuration I-cavity in the transition from a stable to an unstable inner cavity and measure its transmission spectra. We operate the cavity around a length of $L = 14$ mm, where both inner and outer cavity are close to 2-fold frequency-degeneracy ($N \sim 2$). The injected beam is mode-matched to and injected in the fundamental mode of the inner cavity.

We start out with a cavity length slightly shorter than $L = 14$ mm, where the inner cavity is thus still dominantly stable. The spectrum at this position, shown in Fig. 9.5a, contains a small bias and some sharp resonances. The sharp resonances represent stable modes living in the inner cavity. This is confirmed by the intensity profile on the mirror where the power is dominantly localized on the dimple. The bias in the spectrum indicates the onset of the unstable regime.

Figures 9.5b-d show how the spectrum changes if we increase the cavity length such that the inner cavity becomes unstable. Let us discuss this sequence.

The first remark is that the closer we get to instability of the inner cavity the lower becomes the number of sharp resonances in the spectrum. We can explain this as higher order modes become unstable first and only the lower order modes remain.

A second remark concerns the two broad “clumps” per free spectral range, which become more pronounced the closer we come to instability. This is a clear demonstration of the increased coupling to the outer cavity. The two clumps actually consist out of many modes in the almost frequency-degenerate ($N = 2$) outer cavity; the even $(n+m)$-modes are located in one clump and the odd modes in the other.

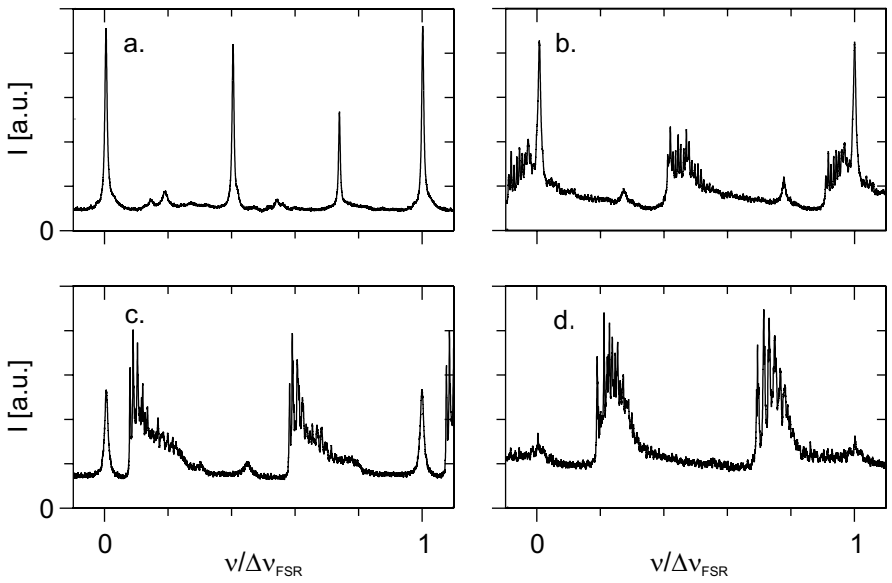

Figure 9.5: *Spectra in the transition from a stable to an unstable inner configuration II-cavity. In figure (a) the cavity is operated at $L = 14$ mm. The cavity length is increased stepwise in consecutive figures to: (b) $\Delta L = 0.11$ mm, (c) $\Delta L = 0.24$ mm and (d) $\Delta L = 0.4$ mm.*

As a third remark, we want to stress that the bias becomes more dominant for a more unstable inner cavity. The bias indicates the presence of many spectrally broad modes, which can no longer be resolved. The origin of this spectral broadening could lie in the fact that these modes presumably encounter more losses, possibly due to the physical transition from the convex to the concave part of the mirror. On the other hand, this does not seem very likely as interferograms indicate that the transition is smooth. Another reason might be that the phases acquired by light in the inner and outer cavity are different so that they interfere destructively when they recombine.

At $L = 14.4$ mm, we are clearly in the regime where we inject in the inner cavity and couple to the outer cavity, since we dominantly excite modes in the outer cavity. This is confirmed by the intensity distribution on the mirror, which is now no longer localized on the dimple but also spread over the outer cavity. We conclude that we are able to couple the inner with the outer cavity, but are unable to spectrally resolve the excited modes.

9.5.2 Cavity finesse, average throughput and the number of hit points

It takes time for chaos to develop and a sufficient number of hits on the mirror, especially on the dimple, is needed. The number of hit points on the mirror can be deduced from the cavity finesse. However, as shown in the previous Section, for some configurations the resonances in the spectrum cannot be resolved and the number of hit points still remains unknown. Especially for this regime, we introduce here a new method to derive the *average*

number of hit points from the "spectrally-averaged" throughput. To test this method, we will first determine the number of hit points of an uncoupled *inner* resonator. Next, we will study an uncoupled *outer* cavity of which the spectral resonances can be resolved. Finally, the new method will be applied to a resonator of which the inner and outer cavity are coupled and the resonances cannot be resolved. The first experiment is performed on a configuration I-cavity, whereas the second and third experiment are performed on a configuration II-cavity.

In the first experiment, we inject a stable inner resonator with a beam mode-matched to the lowest order mode. The configuration I-cavity is operated at a cavity length $L = 13$ mm. The intensity profiles of the modes on the dimple are nice Hermite-Gaussian-modes, as expected for a stable resonator. During alignment of the cavity, the finesse was found to be very sensitive to the exact injection on and alignment of the mirrors. This we also observed in Chapter 7 and is possibly caused by the periodic structure of the roughness on the surface of the substrate. After optimizing the injection, a cavity finesse $F = 670$ is found. This makes the number of hit points on each mirror $F/2\pi = 107$.

In the second experiment, we consider an uncoupled stable outer cavity. We operate a configuration II-cavity at a cavity length $L = 6.6$ mm, which is close to the 4-fold frequency-degenerate point ($N \sim 4$). Off-axis injection at a proper angle excites a corkscrew-like ring-mode, which does not hit the dimple, but retraces its path in the outer cavity. These ring-modes (in the outer cavity) have a finesse of $F = 650$, making the number of hit points on each mirror $F/2\pi = 105$. All resonances can be resolved and have the same spectral width, which indicates that the modes experience identical losses.

We use this second spectrum to demonstrate the validity of our alternative method (see also Section 2.3) to determine the number of hit points. The measured average spectral throughput through one mirror (= average power in a FSR divided by the transmitted power behind first mirror) is 9.4 %. The rest of the light is transmitted by the opposite mirror ($\sim$ 10 %) or scattered out of the resonator ($\sim$ 80 %). We also know that for every hit on a mirror only 8×10^{-4} of the incident power is transmitted. It thus takes on average $9.4 \times 10^{-2}/8 \times 10^{-4} = 120$ hits per mirror before the light has leaked out. As this is comparable to the value $F/2\pi = 105$ obtained earlier, we conclude that the spectrally-averaged throughput provides us with the correct number of hit points and forms an alternative method for the number of hit points deduced from the cavity finesse.

To demonstrate that this new method can be of great benefit in situations where not all spectral resonances can be resolved, we perform a third experiment. We now inject light in a resonator with an unstable inner cavity, for which we chose a configuration II-cavity operated at a cavity length $L = 6.6$ mm. The unstable inner cavity magnifies the input beam and spreads the light over the outer cavity. The inner and outer cavity are now coupled but not all trajectories experience identical losses. This is reflected in the spectrum, which shows an offset, where the resonances cannot be resolved, and on top of that some sharp resolvable resonances. The highest measured cavity finesse of a sharp resonance is $F = 400$, suggesting that the number of hit points on each mirror is $F/2\pi = 65$ (for these modes). Application of our alternative method also reveals information about the modes in the spectral offset, which cannot be resolved in the spectrum. From the measured average spectral throughput of 1.1 %, we deduce an average number of hit points on a single mirror of only $1.1 \times 10^{-2}/8 \times 10^{-4} = 14$. The "average" mode thus hits the mirror a factor $4-5$ times less than the modes of which we can measure the cavity finesse directly. This shows once more that the various modes

experience different losses in a coupled resonator.

In the light of chaos, not only the number of hit points on the outer mirror but also the number of hits on the dimple is important. The ratio between the two is linked to the Gouy phase θ_0 of the outer cavity. The relation between the (integer) number of round-trips N (equivalent to the number of hit points on one mirror before the ray retraces its tracks) and the Gouy phase is given by $N = 2\pi/\theta_0$. For the above configuration the Gouy phase is $\theta_0 = 1.14$, and thus not a true fraction of 2π, but, naively speaking, the number of hit points on one mirror before the ray comes close to its initial position is $2\pi/\theta_0 \approx 5-6$. So if a ray is bounced out of the inner cavity into the outer cavity it takes roughly $5-6$ mirror hits before the ray is again injected into the inner cavity. For a total number of hit points of typically 14, the dimple will be hit only $2-3$ times.

We conclude by stating that our new method, based on a measurement of the average spectral throughput, reveals important information about the number of hit points for modes that cannot be spectrally resolved. We find that the average number of hit points on the mirror in the regime where the inner and outer cavity are coupled is typically only 14. The number of hit points on the dimple is even smaller ($2-3$ hits), and is very likely too small for chaos to develop.

9.5.3 Position of the injection beam

To check the influence of the position of the injection beam on the cavity dynamics we inject on various (off-axis) positions in one transverse plane. We did so for both a stable and an unstable inner cavity, and monitored both the spectrum and the intensity distribution on the back mirror.

Unstable inner cavity

We operate the configuration II-cavity at a cavity length $L = 2$ mm, for which the outer cavity is close to an 8-fold frequency-degenerate point ($N = 8$) and the inner cavity is unstable. For injection in the outer cavity at $\Delta x = 0.56$ mm relative to the mirror center, 8 clumps of modes are observed in the spectrum shown in Fig. 9.6a. The origin of these clumps lies in the fact that the spectrum is dominated by the frequency-degenerate outer cavity ($N = 8$). On the mirror, we indeed observe an ellipse of bright hit points in the outer cavity, bypassing the convex inner part. As the modes are degenerate, individual modes within each clump cannot be spectrally resolved and the cavity finesse cannot be determined. However, from the average spectral throughput we can deduce that the average number of hit points on one mirror for a typical mode is 70.

When we inject closer to the dimple, at $\Delta x = 0.38$ mm, we observe an elliptic ring-structure around the dimple. Fig. 9.6b shows the spectrum in which we still observe 8 clumps of modes, but the clumps are now broader and contain more structure. In each clump there is one sharp dominant resonance on the right side and many more modes with roughly identical peak transmission. The dimple clearly influences the modes in the outer cavity and partly breaks the degeneracy of the modes. The finesse of the sharp resonances is still $F = 670$, and the number of hit points on the mirror for this mode is thus $F/2\pi = 107$. The number of

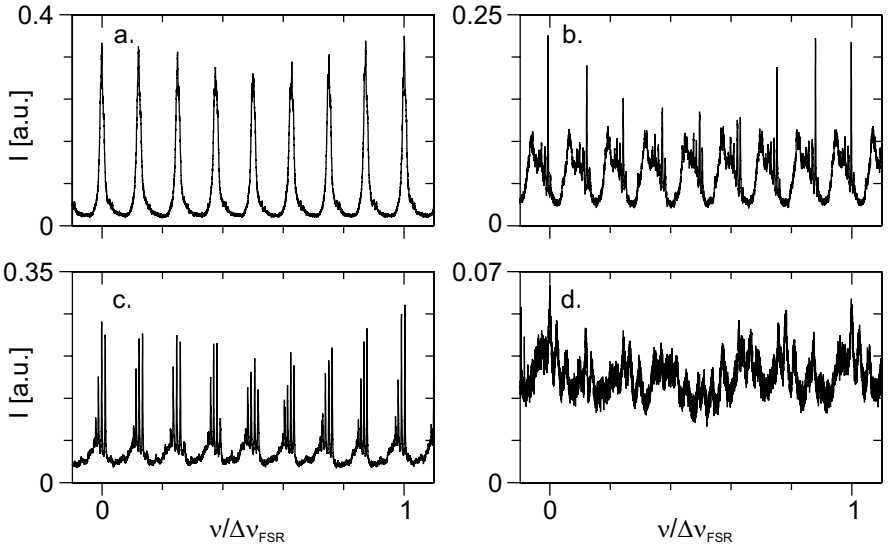

Figure 9.6: *Spectra for various positions of injection into a configuration II-cavity. The resonator is operated at a cavity length of $L = 2$ mm, where the inner cavity is unstable. The outer cavity is close to 8-fold frequency-degeneracy. The outer cavity is injected (a) $\Delta x = 0.56$ mm from the center of the mirror, (b) $\Delta x = 0.38$ mm, (c) $\Delta x = 0.30$ mm, and (d) $\Delta x = 0$ mm, respectively.*

mirror hits found from the average spectral throughput is 60. The discrepancy between these two numbers shows that some modes are more lossy than others.

Injection at $\Delta x = 0.30$ mm from the center of the mirror shows again a ring-structure around the dimple. Groups of modes are still observed in the spectrum Fig. 9.6c. In each clump we can now easily distinguish $4-6$ equally spaced modes. Taking a closer look at some of these resonances we observe a splitting of the modes. This might indicate that also other resonances are still degenerate and consists out of more modes. The finesse of such sharp resonances is $F = 620$, and the number of hit points on the mirror for these modes is thus $F/2\pi = 100$. The average number of hits on the mirror derived from the spectrally-average throughput is 50.

For on-axis injection of the inner cavity, at $\Delta x = 0$, the intensity distribution on the mirror shows that light is spread over both the inner and outer resonator, with a darker fringe in between. We observe an offset in the spectrum (Fig. 9.6d) with some finer structure on top of it. Most excited modes can not be resolved. The few sharp resonances in the spectrum that can be resolve yield $F/2\pi \approx 50$. The average number of hit points, found from the average transmitted power in the spectrum, is 28. As we are close to an 8-fold frequency-degeneracy, the number of hit points N in the outer cavity needed before a ray is reinjected into the inner cavity is $N = 8$. For a total number of hit points on the mirror of 28, the dimple is hit only $3-4$ times.

In summary, we have observed that already for injection at $\Delta x = 0.38$ mm away from the center of the cavity the influence of the inner cavity is felt; the losses increase and the

frequency-degeneracy in the spectrum is broken. As soon as a dominant part of the injected light hits the unstable inner cavity, resonances in the spectra are hard to resolve, which makes it difficult to deduce information from the spectrum. The number of dimple hits is again $3-4$.

Stable inner cavity

Next, the influence of the position of injection on the cavity dynamics is investigated for a cavity with both a stable inner and outer cavity. The configuration I-cavity is operated at a cavity length of $L = 12$ mm, where the inner cavity is close to a 4-fold frequency-degeneracy ($N = 4$).

First, we inject just outside the dimple and observe two bright spots on the left and right side of the dimple and a vague background. The spectrum for this position of injection (Fig. 9.7a) shows an offset and on top of that a quasi-periodic structure ($\sim$ 20-fold). When we inject on the dimple (Fig. 9.7b), the offset in the spectrum has disappeared and instead we observe 4 clumps of resonances in the spectrum, which indicate the 4-fold frequency-degeneracy of the inner cavity. The intensity profile on the mirror is indeed localized on the dimple and the light is thus confined to the stable inner resonator.

Injection on the other side of the dimple results in a spectrum with an offset and on top of that a 7-fold periodic structure, see Fig. 9.7c. On the mirror, we now observe 12 hit points on the concave part of the mirror and some hit points on the convex part, which cannot be pinpointed exactly, due to a limited imaging resolution. This intensity information (> 12 hit points) combined with the 7-fold structure in the spectrum indicates that the number of longitudinal round-trips that are needed before the ray returns on itself equals $N = 14$ [21]. This means that there must be $(14-12) = 2$ hits on the convex part of the mirror. The number of transverse "round-trips" K the orbit makes before closing cannot be deduced directly from our experimental observations. We know, however, that K should be an even integer to comply with the 7-fold spectral structure. A calculation of the overall Gouy phase $\theta_{\text{overall}} = 2\pi K/N$ sheds more light on this problem.

The overall Gouy phase depends on the number of hits on the inner and outer part of the bifocal mirror and is the weighted sum of the Gouy phase of the inner and outer cavity, which is in our case $\theta_{\text{overall}} = \theta_{\text{in}}/7 + (6\theta_{\text{out}})/7$. The Gouy phase of the inner cavity is roughly $\theta_{\text{in}} = 2\pi/4 = 1.57$, whereas the Gouy phase of the outer cavity $\theta_{\text{out}} = 2.95$ for the corresponding cavity length. This results in an overall Gouy phase $\theta_{\text{overall}} = 2.75$. The calculated overall Gouy phase should thus be equal to $2\pi K/14$, which means that $K = 6$.

The existence of this $K/N = 6/14$-point is surprising. For a cavity without dimple and a specific cavity length, one Gouy phase determines all cavity dynamics and $K/N = 6/14$ and $K/N = 3/7$ describe identical physics. The description of frequency-degenerate points in a bifocal cavity is, however, more complicated. For one specific Gouy phase (*e.g.*, $\theta_0 = 2\pi 3/7$), the sequence of hit points on both cavities can be different, which is expressed by $K/N = 6/14$ and $K/N = 3/7$. It is important to note that the orbit described by $K/N = 6/14$ cannot be described by two $K/N = 3/7$-orbits.

We conclude that for a coupled stable inner and outer cavity, an offset appears in the spectrum filled with modes that cannot be resolved. Also for coupled stable cavities, frequency-degenerate points exist, but the Gouy phase does not uniquely define the trajectory.

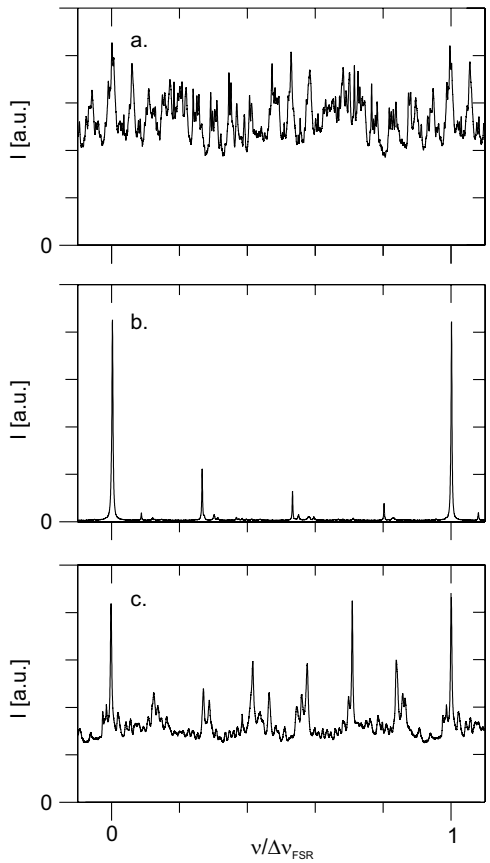

Figure 9.7: *Spectra for various positions of injection of a configuration I-cavity. The cavity is operated at a cavity length of $L = 12$ mm, where the stable inner cavity is close to 4-fold frequency-degeneracy. The position of injection as compared to the mirror center Δx is for (a) $\Delta x = -0.12$ mm, (b) $\Delta x = 0$ mm, and (c) $\Delta L = 0.17$ mm, respectively. Note the (quasi-periodic) structure in both (a) and (c), where the rays hit both the inner and outer cavity.*

9.6 Transmission patterns

9.6.1 Speckle patterns

Important information can also be obtained from the transmission profiles. When we inject the unstable inner cavity, the light spreads out over the convex and concave part of the bifocal mirror. Close to frequency-degeneracy of the outer cavity, circular structures dominate the speckled pattern as shown in Fig. 9.8a. These circular structures are the Hercher fringes introduced in Chapter 4. We will concentrate, however, on the nondegenerate case as shown in Fig. 9.8b. The patterns can be observed best for fixed cavity length, *i.e.*, when the scanning

of the cavity length is stopped.

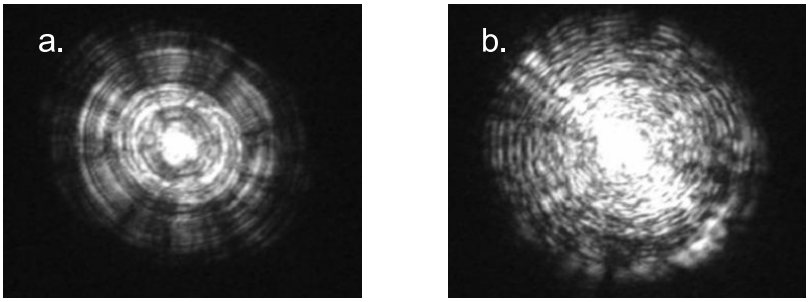

Figure 9.8: *Intensity profiles on the mirror of a configuration I-cavity for a fixed cavity length (no scanning) (a) operated at $L = 14.3$ mm, where the outer cavity is close to 2-fold frequency-degeneracy ($N \approx 2$) and (b) away from a frequency-degenerate point at $L = 17.3$ mm. Close to frequency-degeneracy Hercher-fringes dominate the speckle pattern.*

We encounter the speckled patterns not only for short cavity lengths, but also for the longer ones. On first sight, the patterns appear to be random, but a closer look shows rotational symmetry. Such intensity profiles with a rotational symmetry were also observed for a similar, but uncoupled system, introduced in Chapter 8. We have demonstrated there that Laguerre-Gaussian (LG) eigenmodes form the natural basis of the uncoupled system. Similar speckled patterns were observed and associated with a (coupled) superposition of many excited LG-modes. The patterns in the coupled system, presented in this Chapter, have the same flavor.

The randomness and structure of the speckles in the patterns imply that many unperturbed LG-modes are involved. The speckle size or, equivalently, the spatial period can be attributed to the highest-order mode m involved. The connection between mode number m involved and the size of the speckles Λ_m is $m = (4w/\Lambda_m)^2$ [12] with w the waist of the fundamental mode. The typical size (FWHM) or correlation length of a speckle in the pattern is measured to be $20 - 50$ μm. For $w = 40$ μm we thus find that the highest-order mode involved has a mode number $m = 10$ to 60.

A polarizer behind the resonator gives more insight into the speckle patterns. The transmission axis parallel to the input polarization results in a typical speckle pattern as shown in Fig. 9.9a. We observe again some rotational symmetry in the patterns. Rotation of the output polarizer over 90° (transmission axis perpendicular to the input polarization) shows, to our surprise, that light is still transmitted through the polarizer. Obviously, the resonator changes the polarization of the light and acts as a depolarizer. Fig. 9.9b, with crossed polarizers, is different from Fig. 9.9a; the light is spread more homogeneously over the mirror and structure of the speckles is more grainy.

The difference in intensity distributions for both polarizations can be analyzed more quantitatively by averaging over many intensity realizations in a free spectral range. The comparison is then easier as we are less sensitive to vibrations that change the cavity length on a

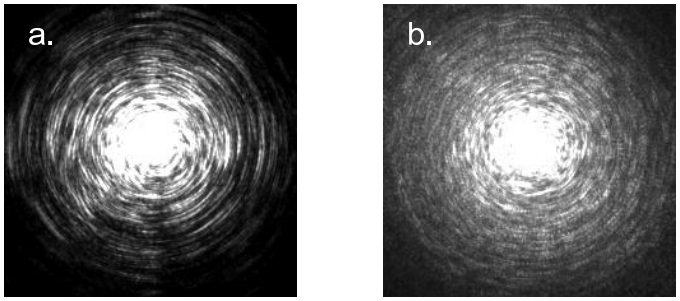

Figure 9.9: *Intensity profiles on the mirror behind a polarizer with its transmission axis (a) parallel and (b) perpendicular to the input polarization. The configuration II-cavity is operated in between two frequency-degenerate points at a cavity length $L = 1.8$ mm. The images correspond to an area of 1×1 mm^2 on the composite mirror. The dimple is overexposed.*

sub-wavelength scale over time. Disadvantage of this method is that the speckles are averaged out and that we loose intensity information on smaller length scales. We achieve the averaging by scanning the resonator with a piezo over a few wavelengths. Cross-sections of these averaged intensity patterns are shown in Fig. 9.10. The intensity is highest in the center of the dimple, where we inject, and decreases closer to the edges of the mirror. This decrease is strongest for the parallel case. The distribution for polarization perpendicular to the input polarization is more uniform. The ratio of these two polarized intensities decreases from 200 in the center to ~ 70 at $\rho = 0.5$ mm. 2D-images of the intensity distributions show that the total (area-integrated) transmitted power is 75 times stronger for the polarization parallel to the input polarization than for the perpendicular polarization. This ratio is also found from the spectra of both polarizations.

9.7 Discussion and recommendations

In this Chapter, we have presented a preliminary experimental investigation of a novel type of open optical resonator. This resonator has been shown to be able to couple the inner and outer cavity. The number of hit points in the inner (unstable) cavity was found to be limited to typically only $3-4$. For chaos to develop in our 3D-cavity more hits are probably needed.

Rays that remain solely within either the stable inner or outer cavity were observed to do so during about $60-110$ round-trips. This number is large enough to distinguish individual modes in the optical spectrum. In the coupled regime, where chaos might develop, the number of hit points, however, decreases drastically and resonances in the spectrum become hard to resolve. This makes it difficult to perform the statistics that is needed to show the presence of chaos in our experiment. The reason for the observed broadening might be that light in the inner and outer cavity acquire a different phase and interferes destructively.

Our first recommendation concerns the coupling of the inner and the outer cavity, which is up to now relatively modest. For coupled systems, it is obvious that the phase plays a

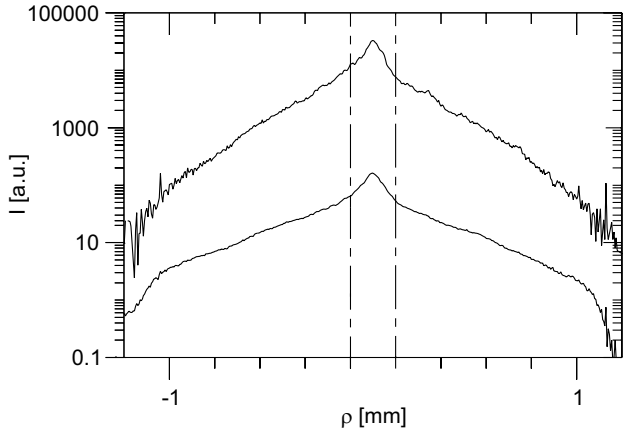

Figure 9.10: *Cross-sections of intensity profiles averaged over many realizations in a free spectral range. The upper and lower curve represent the intensity distributions observed behind a polarizer oriented parallel and perpendicular to the input polarization, respectively. The configuration II-cavity is operated at a length of* $L = 1.8$ *mm. The two dotted-dashed lines indicate the position of the dimple,* ρ *ranging from -0.1 to 0.1 mm.*

crucial role [12]. As our system is a coupled transverse *multi*-mode system, many phases are involved. To adapt the phase of the inner cavity to the outer cavity, we propose a bifocal mirror of which the dimple can be axially displaced on a sub-wavelength scale. Proper matching of the optical phases in the inner and outer cavity might increase the coupling between the two cavities.

Our second recommendation concerns the presence of corkscrew-like (ring)modes that live solely in the outer cavity. Although these modes do not contribute to chaos, they are still present in the spectrum and make it harder to resolve individual resonances. An azimuthal obscuration inside the outer cavity will block these ring-modes much more than the wanted 2D-modes that hit the dimple and contribute to chaos. With such an obscuration, the spectrum should contain less resonances but relatively more resonances that might demonstrate chaotic behavior. The proposed obscuration will also break the rotation symmetry of our cavity; a symmetry that could frustrate some types of chaos.

9.8 Acknowledgement

We thank Andrea Aiello for his initial work on this topic and for the many discussions.